energies

MDPI

Review

Computer Vision and Machine Learning Methods for Heat Transfer and Fluid Flow in Complex Structural Microchannels: A Review

Bin Yang [1], Xin Zhu [1], Boan Wei [1], Minzhang Liu [1,*], Yifan Li [1], Zhihan Lv [2] and Faming Wang [3]

[1] School of Energy and Safety Engineering, Tianjin Chengjian University, Tianjin 300384, China
[2] College of Art, Uppsala University, s-75105 Uppsala, Sweden
[3] Department of Biosystems, Katholieke Universiteit Leuven, BE-3001 Leuven, Belgium
* Correspondence: liuminzhang@tju.edu.cn

Abstract: Heat dissipation in high-heat flux micro-devices has become a pressing issue. One of the most effective methods for removing the high heat load of micro-devices is boiling heat transfer in microchannels. A novel approach to flow pattern and heat transfer recognition in microchannels is provided by the combination of image and machine learning techniques. The support vector machine method in texture characteristics successfully recognizes flow patterns. To determine the bubble dynamics behavior and flow pattern in the micro-device, image features are combined with machine learning algorithms and applied in the recognition of boiling flow patterns. As a result, the relationship between flow pattern evolution and boiling heat transfer is established, and the mechanism of boiling heat transfer is revealed.

Keywords: computer vision; machine learning; heat transfer; fluid flow; complex structural microchannels

Citation: Yang, B.; Zhu, X.; Wei, B.; Liu, M.; Li, Y.; Lv, Z.; Wang, F. Computer Vision and Machine Learning Methods for Heat Transfer and Fluid Flow in Complex Structural Microchannels: A Review. *Energies* **2023**, *16*, 1500. https://doi.org/10.3390/en16031500

Academic Editor: Fernando Sánchez Lasheras

Received: 30 December 2022
Revised: 17 January 2023
Accepted: 31 January 2023
Published: 2 February 2023

1. Introduction

With the rapid development of microelectronics technologies, large-scale integrated circuits, and high-speed computers, high power, high integration, and miniaturization have become the main development trends of electronic devices [1,2]. However, as electronic device miniaturization and integration progress, heat generation per unit volume increases dramatically. During operation, the device must withstand an ultra-high heat flux of 6.5–50 MW/m^2 [3], which poses a challenge to the device's cooling systems. If the surface temperature of the micro-device cannot be reduced quickly and effectively, it will reduce the working performance and even burn the device, severely limiting the development of microelectronic devices. Traditional cooling technologies (air cooling, liquid cooling, and so on) are no longer capable of dissipating the high heat flux in millimeter- or even micrometer-scale devices [4]. As a result, the heat dissipation of micro-devices with high heat flux has become an urgent problem that must be solved.

Microchannel boiling heat transfer (BHT) is currently one of the most effective methods for removing high heat loads from micro-devices [3]. The flow pattern changes continuously during the BHT process inside the microchannel due to the different drynesses along the direction of fluid flow. BHT flow patterns in microchannels differ from those in conventional scale channels. Bubbly flow, slug flow, annular flow, stratified flow, mist flow, and other flow patterns are examples of flow patterns in conventional scale channels [5]. There are three flow patterns in the process of the microchannel BHT: bubbly flow, elongated bubbly flow, and plug/annular flow [6]. At the same time, there are complex nonlinear flow pattern transition regions in microchannels, such as the transition from chaotic bubbly flow to slug flow, and the transition from slug flow to annular flow [7,8]. In a two-phase system, different flow structures and flow patterns correspond to different heat transfer mechanisms. Nucleate BHT and forced convective boiling heat transfer (CBT) are the

most common types of heat transfer in microchannels [9,10]. The emergence of elongated bubbly flow and plug/annular flow will inhibit nucleate boiling in the channel, and the BHT process will change from nucleate BHT to forced CBT [11]. As a result, accurate identification of the evolution of flow patterns during the BHT process in microchannels is the premise for revealing the mechanism of enhanced BHT of the microchannel, which is critical for microchannel design.

The diversity of flow patterns and the limitations of detection methods all have an impact on flow pattern recognition in the boiling process. As a result, heat transfer prediction models based on flow pattern evolution have large errors. It is difficult to improve the accuracy of flow pattern recognition in complex structural microchannels. The combination of computer vision and machine learning technologies with the rapid development of artificial intelligence technologies provides a new method for flow pattern and heat transfer identification in microchannels. Computer vision technology uses the image information captured by the camera to identify and analyze the object via a computer, which has intuitive and contactless characteristics. Machine learning is a multi-field interdisciplinary discipline, employs algorithms to analyze data, learns from the date, and then predicts targets. It possesses automatic learning, high accuracy, and strong practicability features. Machine learning and computer vision techniques have also achieved excellent recognition accuracy and the effective extraction of important image features in popular areas of image recognition, such as agriculture [12], medicine [13], geography [14], food processing [15], urban planning [16], manufacturing [17], and engineering [18].

This review paper first summarizes the visualization research on flow pattern recognition in the boiling process of complex microchannels. It includes the visualization study of some novel micro-structures and different wettability surfaces, as well as the study of flow pattern recognition in microchannels using computer vision techniques, followed by a summary of the application of machine learning in flow pattern recognition. It will lay the groundwork for establishing a link between flow pattern evolution law and BHT, as well as providing a framework for future research on the BHT mechanism.

2. Monitoring Methods by Visualization

Boiling heat transfer in microchannels has received a lot of attention in the field of miniature electronic devices because of its good heat dissipation effect [3]. Many studies have concentrated on the heat transfer mechanism in flow boiling [19], bubble motion [20], flow boiling instability [19,21], and critical heat flux (CHF) [22]. The BHT mechanism in microchannels is closely related to flow morphology and bubble behavior. Understanding flow boiling in microchannels can be improved by visualizing high-speed flow. In recent years, a large number of researchers have used high-speed photographic cameras to visualize flow boiling in microchannels. Meanwhile, with the rapid development of computer vision technology, some researchers have used computer vision technology to perform image processing on the raw images captured by high-speed cameras. The mechanism of enhanced BHT of micro-structures was developed by accurately identifying the evolution law of the flow pattern during flow boiling.

2.1. Visualization of Flow Patterns

Suo and Griffith [23] investigated the flow patterns of capillary channels and identified three distinct flow modes: bubby flow, slug flow, and annular flow. According to Kandlikar et al. [6], the process of microchannel boiling involved three major flow patterns: bubbly flow, elongated bubbly flow, and slug/annular flow. Thome et al. [24] summarized the main flow states in microchannels, which included mist flow and stratified flow, in addition to the three basic flow patterns mentioned above (see Figure 1). Other flow patterns represented sub-states or transition patterns between these main states. Although nonlinear flow pattern transition regions were complex in terms of microchannels, classical flow patterns such as bubbly flow, slug flow, and annular flow were easily identified. The current lack of

uniform standards for microchannel flow patterns makes it difficult to establish a common method for studying microchannel BHT under a wide range of conditions.

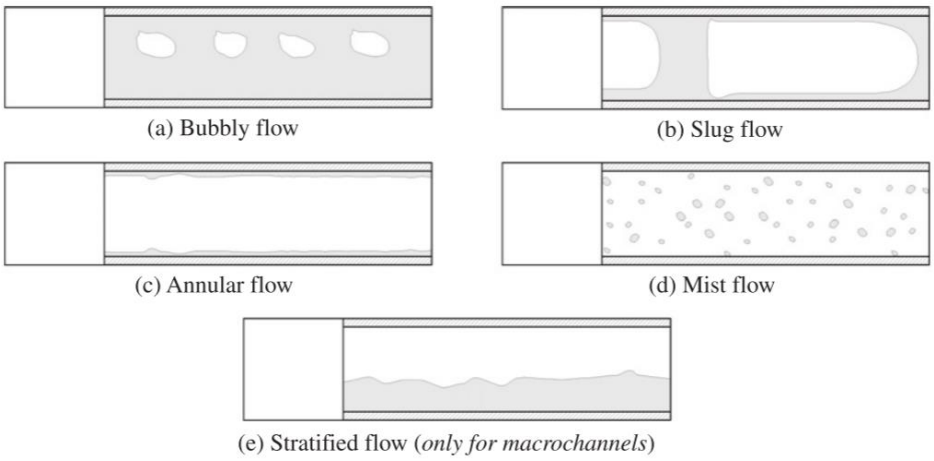

Figure 1. Five flow patterns [24].

Flow regime maps are frequently used to determine flow patterns in the boiling process under various experimental conditions, as well as flow pattern transition conditions. Flow regime maps with vapor and liquid mass flux, as well as steam dryness, were plotted by Charnay et al. [25], Mahmoud et al. [26], and Ong and Thome [27]. Thome et al. [24] observed that the boundary lines of these flow regimes depended on the working fluid, operating pressure, and channel geometry. They proposed a set of comprehensive development suggestions for flow pattern maps, which can represent the equilibrium state of a two-phase flow structure. There is no unified standard for flow regime maps of two-phase flow in microchannels at the moment, and there have been few studies on flow regime maps suitable for multiple microchannel structures.

2.2. High-Speed Visualization of Different Microchannel Structures

In recent years, some new microchannel structures have been designed, and microstructures such as micro-fins [28], pin fins [29,30], artificial grooves [31], and serrated structures [32] have been established in microchannels to improve heat exchange. Others, such as square microchannels [33], divergent microchannels [34], and trapezoidal microchannels [26], try to improve heat transfer by increasing the heat transfer area and strengthening bubble nucleation. Bubble motion is affected by solid boundaries inside complex microchannels, and different geometries can result in some unusual flow patterns.

2.2.1. Microchannels with Increasing Heat Transfer Area

Using high-speed cameras, researchers have investigated the variations in flow patterns in rectangular microchannels with large depth–aspect ratios. Zhou et al. [35] investigated subcooled flow boiling in a rectangular microchannel with a high aspect ratio and unilateral heating. A high-speed camera was used to observe the flow pattern, and they discovered that the flow pattern was primarily elongated bubbly flow, and the liquid film evaporation mechanism dominated the entire test section due to bubble elongation, transient local drying, and rewetting. Krishnamurthy et al. [9] observed an isolated bubble region, a bubble interaction region, a multiple flow region (bubbly/slug flow region), and an annular flow region in a rectangular microchannel with micro pins, and they provided a flow pattern diagram with the boiling number and dimensionless distance as coordinates. Liao et al. [36] used image acquisition to investigate the flow boiling and heat transfer characteristics of FC-72 in rectangular microchannels. The results showed that at the start of the boiling, bubbles were formed at the edges of the nucleated fin holes, and then steam was formed in the nucleated hole and sprayed into the main flow. Eventually, the large

steam blocks formed around the micro-fins. Flow patterns such as bubble flow, block flow, droplet/block flow, droplet flow, and annular flow can be observed as the heat flux increased gradually. Zhang et al. [33] conducted flow boiling experiments in a square microchannel using ethanol as the working medium. They measured the thickness of the transient liquid film during flow boiling using a laser confocal displacement meter (LFDM). The flow boiling process can be divided into three regions based on the variation of the wall temperature and liquid film thickness. These regions are the liquid plug region, the elongation bubble region, and the dry region. Yang et al. [37] created a novel square-section microchannel heat sink. For different inlet vapor qualities, a high-speed camera discovered four major flow patterns: bubbly flow, slug flow, churn flow, and annular/wave flow. Feng and Zhang [38] investigated the two-phase flow of a nitrogen carboxymethyl cellulose (CMC) solution and a nitrogen–water solution in a square horizontal microchannel. They identified the unique behavior of the bubbly flow and churn flow using flow patterns captured by a high-speed camera. The front of the bubble was pointed and long, while the back was flat. Furthermore, when the CMC solution concentration is high, the liquid film is thick, and the apparent gas velocity of the flow pattern transition (slug–slug–annular flow, slug–annular–churn flow) is higher. Cheng and Wu [39] used deionized water as the working medium in flow boiling experiments in novel high-aspect ratio groove-wall microchannels. The groove-wall microchannels had a lower onset of nucleate boiling, a higher heat transfer coefficient, and a lower pressure drop than the flat-wall microchannels. Cheng and Wu [40] photographed the flow boiling process in interconnected microchannels (IM), where nucleating bubbles were easily obtained. However, there was almost no bubbly flow in the plain-wall microchannel (PM), and regular liquid film redevelopment and annular flow alternated in the IM.

2.2.2. Microchannels with Micro Structures

Researchers have created special micro-structures to improve heat transfer in microchannels. Li et al. [41] designed the triangular cavities and rectangular fins for the microchannels. A high-speed camera was used to observe bubbles forming from triangular cavities, expanding upward/downstream at the same time, and eventually forming the annular flow. Lin et al. [34] investigated the CHF and CBT of methanol–water mixtures in an expanding microchannel with artificial cavities. Flow visualization revealed that bubbles typically formed at the artificial cavities and the channel's side wall, confirming the artificial cavity's function. Wu and Cheng [42] investigated the flow boiling of water in a parallel trapezoidal section of a silicon microchannel through visualization. When the BHT was established, the two-phase flow and single-phase flow alternated in the microchannel. Meanwhile, in the microchannel, unusual flow patterns such as bubbly flow, slug flow, and churn flow were observed. Alam et al. [43] used a high-speed flow visualization experiment to compare the BHT and pressure drop characteristics of silicon microcap heat sink and microchannel heat sink in deionized water. Because it could form slug/annular flow earlier, the microchannel heat sink achieved better heat transfer performance at low heat flux. At high heat flux, however, the microcap heat sink performed better, because confining slug and annular flows were dominant, thus delaying the drying stage. Alam et al. [44] used high-speed visualization technology to compare the bubble size, liquid film thickness, and interface properties of SiNW microchannels and conventional microchannels. Image analysis revealed that the mechanisms of bubble growth in the SiNW microchannel and the conventional microchannel differed significantly. Furthermore, the reverse flow velocity in the conventional microchannel was greater than that in the SiNW microchannel. Surface tension dominated in the bubble nucleation and slug/transition flows, while vapor inertia forces dominated in the annular flow, according to force analysis during instantaneous bubble growth.

Prajapati et al. [45] investigated the flow boiling characteristics of microchannels with three different structures: constant-section microchannels, expanding-section microchannels, and segmented-fin microchannels. The constant-section channel at high heat flux

had the most serious bubble clog and backflow problems, which were partially solved in the expanding-section channel. The bubble blockage was completely removed in the segmented channel, allowing the growing bubbles to pass through smoothly and easily. Deng et al. [29] used a high-speed camera to conduct flow boiling experiments on open-ring pin fin microchannels (ORPFM). The ORPFM was discovered to promote the early nucleation of bubbles. The circular cavity and the unique open-ring pin fin structure provided an ideal space for bubble nucleation. Lyu et al. [30] discovered special flow patterns such as liquid island, air pocket, and a conical gas–liquid boiling development zone while conducting boiling/evaporation heat transfer experiments in channels with staggered diamond-shaped micro-fins. Markal et al. [46] investigated the effect of channel expansion on flow boiling characteristics in three types of micro heat sinks, including straight parallel channels, evenly distributed micro-fins, and a reduced number of micro-fins in the flow direction. The expanding channels significantly improved the two-phase heat transfer coefficient when compared to parallel channels and channels with uniformly distributed micro-fins. The decreasing number of micro-fins inhibited the boiling instability significantly, and the pressure drop was lower than that seen with uniformly distributed micro-fins. In the high-saturation region, the expanding channels provided escape routes. As a result, the flow was accelerated and the steam's residence time on the heat transfer surface was reduced.

2.2.3. Other Microchannels

Yin et al. [47] designed an open microchannel and experimented with subcooled flow boiling. The flow characteristics and bubble behavior of various flow patterns were observed using a high-speed charge-coupled device (CCD) camera. The results revealed that flow patterns in the open microchannel differed from those in the closed microchannel, and that stratified flows existed without flow instability. Two types of restricted bubbles were discovered. Li and Wu [48] investigated flow boiling in bidirectional counter-flow (BCF) and unidirectional parallel flow (UPF) microchannels. To observe the two-phase flow, a high-speed camera was used. In contrast to UPF microchannels, the start of nucleate boiling (ONB) in BCF microchannels was shifted from the downstream to the middle region. In the BCF microchannel, the drying phenomenon downstream of the UPF microchannel was well resolved. Lee et al. [49] investigated the effect of the compressible volume position in the closed flow circuit on the two-phase instability during the FC-72 flow boiling in the microchannel heat sink, and the flow transition along the channel was observed using a high-speed camera. Flow instability causes transient flow states such as bubbly flow, slug flow, churn flow, annular flow, mist flow, and even dry out along the channel. Liu et al. [50] performed a visual study on the flow boiling characteristics in small channels, with water as the working medium, and discovered that the merging of the bubbles could result in a small increase in the heat transfer coefficient. Vermaak et al. [51] investigated the flow boiling of FC-72 in horizontal micro/small channels under different gravitational rotation directions. The visualization results reveal that the rotation angle had a significant effect on the performance of the bubble detachment and heat transfer. Hong et al. [52] used visualization experiments to investigate the flow and heat transfer characteristics in ultra-shallow microchannels with two types of structures. The two-phase flow was significantly accelerated because of the parallelogram structure and the unbalanced force exerted on the bubble. Halon et al. [53] investigated the two-phase flow patterns of R245fa in a microchannel array, and a high-speed camera was used to observe four types of two-phase flow patterns, as shown in Figure 2. The first and second flow combinations were intermittent flow and annular flow, respectively. Hong et al. [54] used visualization to investigate the effects of geometrical parameters on bubble growth, coalescence, and elongation. The experimental results revealed that the transverse growth of the bubble was linearly related to RE 3/2 (equivalent spherical radius of the bubble), and was determined by the geometric parameter wc^2hc (wc: channel width; hc: channel depth). The aspect ratio determined the direction and rate of bubble elongation.

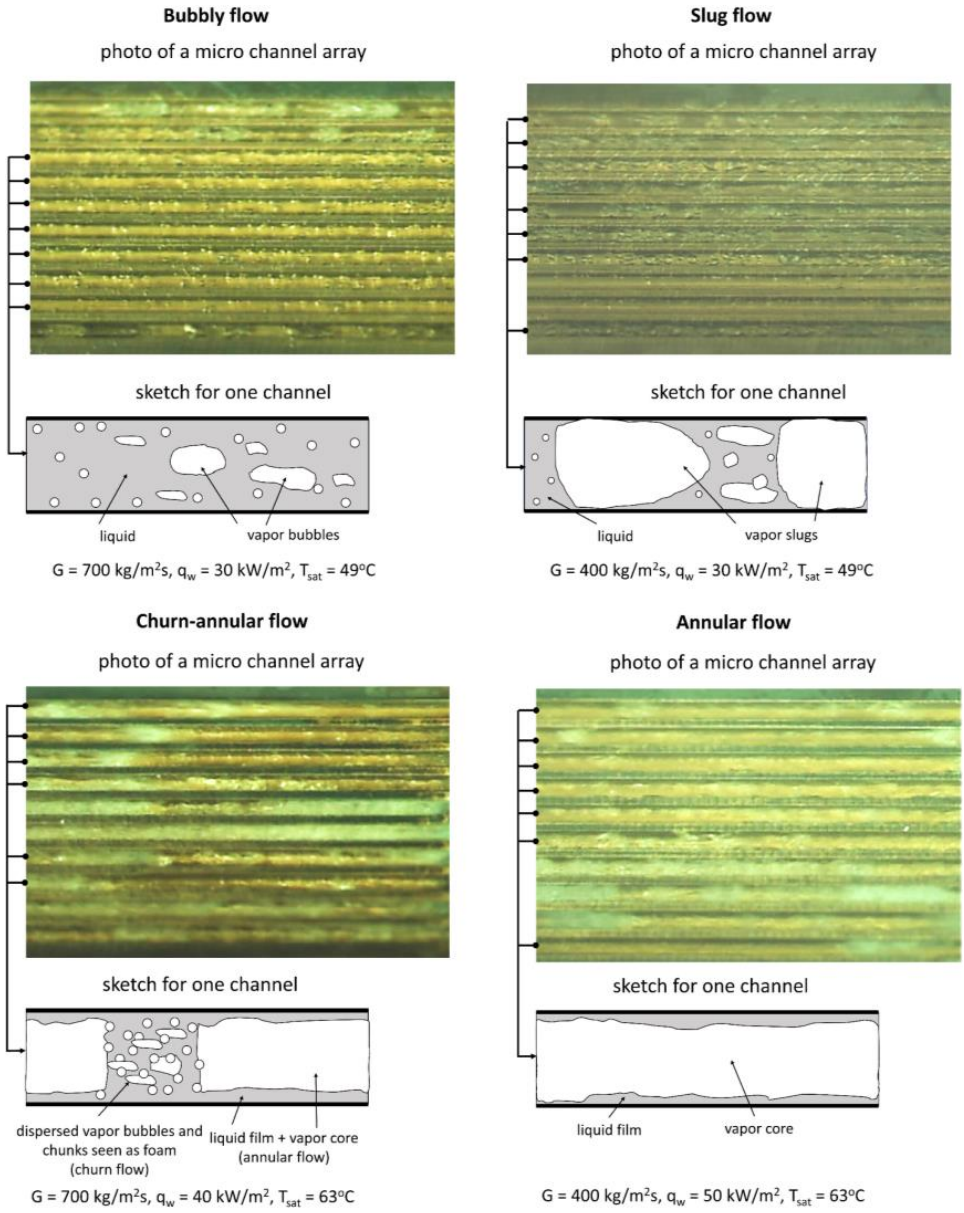

Figure 2. Four flow patterns and schematic diagrams. G—Mass flux in the micro channel (kg/(m^2/s)). q_w—Heat flux (W/m^2). T_{sat}—Saturation temperature (°C) [53].

The randomness and chaos in the evolution of flow patterns were more apparent in microchannels with complex structures, making flow pattern identification more difficult. Furthermore, the variation in the flow pattern could cause the system pressure and temperature to fluctuate, resulting in a random and variable flow structure, making the flow pattern more complex and difficult to measure.

2.3. Visual Study on the Surface Wettability of Microchannels

Aside from structural improvements, the surface wettability of microchannels has received a lot of attention. By adjusting the surface wettability of microchannels, many researchers attempt to improve the heat transfer capacity and reduce flow instability. Zhou et al. [55] used scanning electron microscopy to examine the surface morphologies of microchannels with three different types of surface wettability (super hydrophilic (SHPI) surface, hydrophilic (HPI) surface, and untreated surface). The results show that the degree of bubble nucleation in the SHPI microchannels was significantly higher at the start of the boiling than in the untreated microchannels. The SHPI surface microchannel was found to

have more active nucleation cavities, a high nucleation rate, a large nucleation number, a small bubble departure diameter, and a fast departure frequency, promoting flow and heat transfer in the microchannels. Zhao et al. [56] investigated the heat transfer and pressure drop properties of two-phase flow in three open microchannels: SHPI, HPI, and super hydrophobic (SHPO). In addition, the relationship between flow pattern transformation and two-phase flow boiling performance was investigated. The results reveal that the local dry out in the stratified flow was captured in the HPI microchannels, but not in the SHPI microchannels. At high heat flux, a new trapping bubble was observed in the SHPO microchannel, trapping the vapor and slug film and restricting the rewetting area. Qin et al. [57] investigated the flow boiling characteristics of diamond micro-fin arrays coated with hydrophobic materials experimentally. A high-speed camera was used to photograph the flow pattern and vapor film. Flow boiling in the micro-fins array could be divided into four states as the mass flow rate increased: film boiling, transition from film boiling to nucleate boiling, nucleate boiling, and single-phase convective boiling. During film boiling, transition boiling, and nucleate boiling, the flow boiling performance of diamond micro-fins on hydrophobic and SHPO surfaces was superior to that of bare copper surfaces.

2.4. Application of Computer Vision Technology

Computer vision technology, which is intuitive and non-contact, uses the image information captured by a camera to identify and analyze the target object via the computer. With the rapid advancement of science and technology, computer vision technology now offers a new method for identifying boiling flow patterns in microchannels. Fore et al. [58] used a high-speed camera to identify and study the bubbles of the elastic flow and bubbly flow in the classical two-phase flow of the vertical pipeline, followed by filtering, edge detection, and image binarization of the acquired images, and then extracted the bubble edges and calculated their size. Hanafizadeh et al. [59] used image processing to investigate the effect of flow patterns on heat transfer. The acquired images were first grayed out and an image subtraction algorithm was applied to reduce the background noise by subtracting the background from each dynamic image. A median filter was used to smooth the image boundaries. It was useful for reducing speckles and pepper noise, and removing undesirable blurred edges. The image was converted from grayscale mode to binary mode by thresholding segmentation, and the bubble and slug flows were identified successfully, as shown in Figure 3. Resistance tomography was used by Harrison et al. [60] and Babaei et al. [61] to study the mixing effect of multiphase flow. Huang et al. [62] and Fei et al. [63] used digital image processing technology and computational homology group theory to quantify the behavior of droplet swarms in multiphase flow in direct-contact steam generators, and the coupling relationship between droplet swarms and heat transfer was obtained. The image processing method mainly included the top-hat transform, which suppressed the background of the original image, eliminated noise and enhanced the image; the binarization operation, which aimed to calculate the Betti numbers, and the open operation, which eliminated the individual bubbles or groups of small bubbles represented in the binarized image. The image processing process is shown in Figure 4. The number of droplets and the agglomeration behavior in droplet populations were analyzed quantitatively by the computational homotropy group theory. The evolution of blocks, holes and agglomerates was studied via Betti numbers, and thus the non-uniformity of the droplet population's mixing was characterized. Li and Hrnjak [64] used the video processing method of brightness to measure the plug speed, which was one of the most important characteristics of the plug/bouncy flow, then calculated the plug speed by measuring the speed of the plug head in the frame, corrected the plug speed using video information, and proposed a new correlation formula for predicting the plug speed. Liu and Pan [65] developed a non-invasive method for measuring fluid temperature and two-phase flow regime in microchannels, and the experimental results confirmed that infrared thermography can be used to capture transient flow patterns and fluid temperature along the channel. This is the first study to propose the infrared visualization of two-phase flow patterns

within microchannels. Huang and Thome [66] used a high-resolution infrared camera to measure the bottom temperature of the test section, created a two-dimensional heat map, and calculated the local heat transfer coefficient by solving the three-dimensional heat conduction inverse problem. The experimental results show different trends along the flow direction, and a flow pattern-based model (from the subcooled zone to the circular flow) has been proposed. Korniliou et al. [67] investigated the complex physical phenomenon of two-phase flow boiling in microchannels using a combination of non-invasive infrared thermography and flow visualization, and discovered that the axial expansion of the elongated bubbles along the channel contributes to the flow reversal, dryness in the channel edges, and high-amplitude fluctuations of the temperature and pressure.

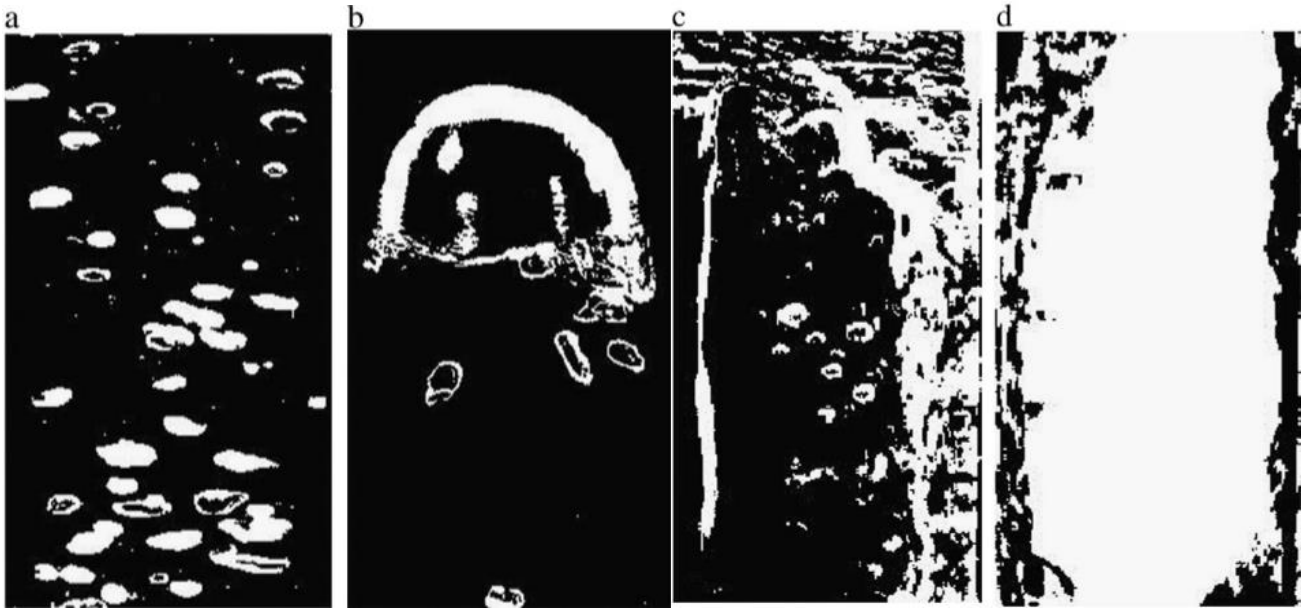

Figure 3. Four main flow pattern images processed. (**a**) bubbly; (**b**) slug; (**c**) churn; (**d**) annular [59].

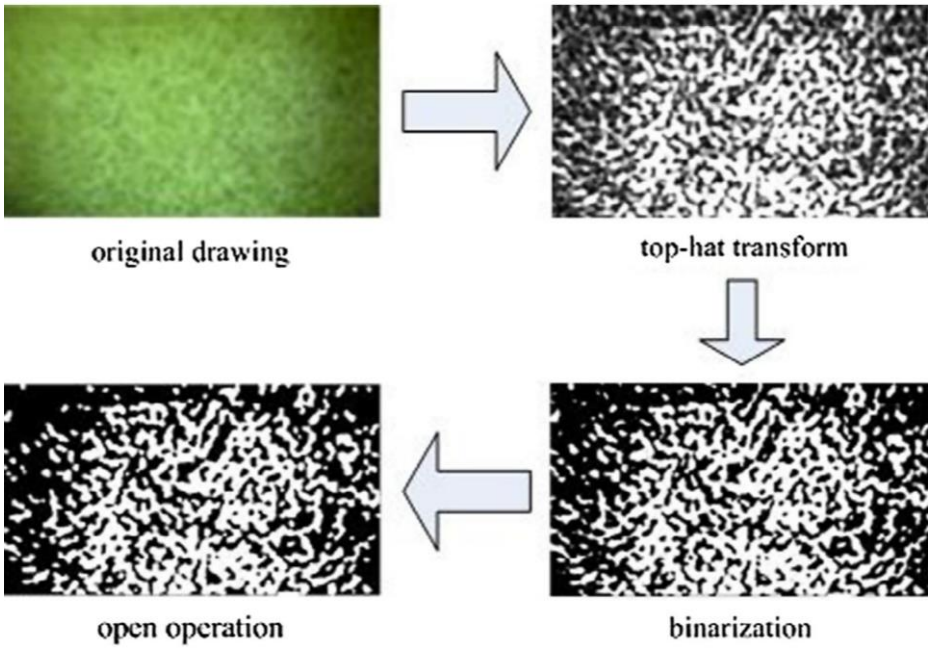

Figure 4. Original diagram of droplet swarm and digital image technology processing diagram in direct-contact steam generator [62].

From the analysis of the above study, it is found that computer vision technology provides a new way to extract quantitative information about the bubble behavior and flow pattern evolution of flow boiling in microchannels, which can provide an important reference for building bubble dynamics models to reveal the interrelationship between flow and heat transfer.

3. Application of Machine Learning in Microchannel Flow Pattern Recognition

3.1. Intelligent Flow Pattern Identification Process Based on Machine Learning

Machine learning is a multi-disciplinary approach that uses algorithms to analyze data, learn from them, and predict a target. Machine learning has the advantages of automatic learning, high accuracy, practicality, convenience, and economy. Machine learning methods provide a new approach to flow pattern recognition. In modeling fluids in microchannels using machine learning, data set creation, feature selection, model tuning, model validation and testing are essential, as shown in Figure 5.

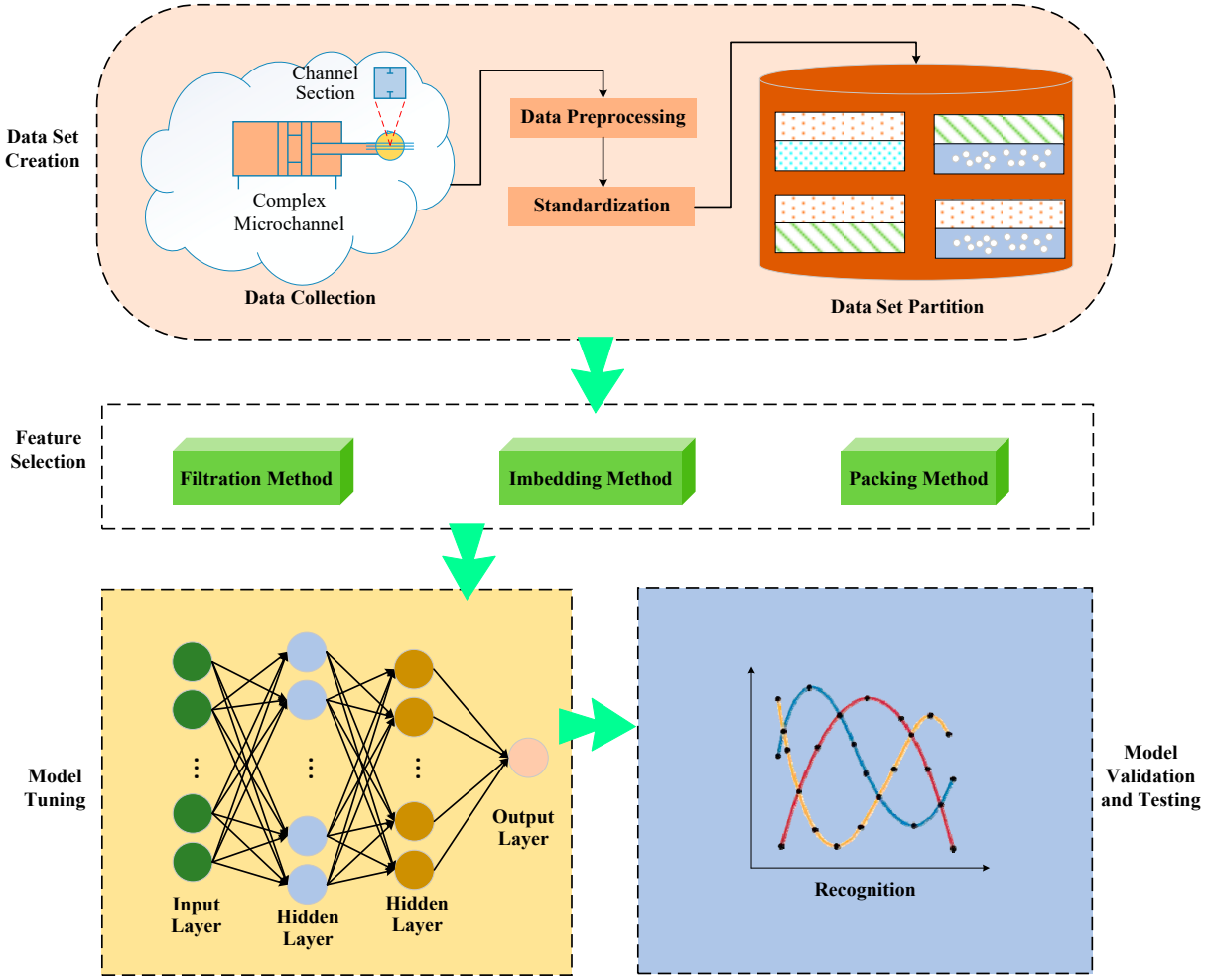

Figure 5. Schematic diagram of the feed-forward network applied to fluid modeling in microchannels.

As shown in Figure 5, the process of flow pattern recognition of multiphase flow in microchannels via machine learning mainly includes data set creation, feature selection, model tuning, model validation and testing.

Firstly, the establishment of the data set is completed through the steps of data collection, pre-processing (including checking the rationality and validity of the data set, missing data, and exception handling), standardization (including normalization and standardization), and data set division. The normalization process can scale the attribute between the

specified maximum and minimum values. Standardization refers to scaling a data set to restrict it to a small and specific interval. The absolute value of the processed data has less difference, and can be negative or positive. Then, the standardized data are divided into a training set, a verification set, and a test set according to set proportions [68]. In the process of establishing a data set, the coverage of the working conditions is particularly important for the performance of the machine learning model, and special attention should be paid when selecting and dividing the data set.

Secondly, feature selection is key to the quality of prediction results. An excessive number of features may lead to overfitting in the training process; conversely, a lack of sufficient information is not conducive to optimizing the training of the model. Selecting high-quality features will directly improve the prediction effect of the model. In addition, when selecting feature parameters, there are two key factors that need to be considered to optimize the model's performance and its ability to express data. One is whether the characteristic parameters will cause divergence; another is whether the typical parameters have a strong correlation with the target output variable. At present, the most common feature selection methods mainly include the filtering method, the embedding method, and the packing method [69–71]. However, the selection of characteristic input parameters of multiphase flow identification largely depends on the user's physical knowledge or experience in screening. Few of the theory-biased selection algorithms above are applied.

Thirdly, model-tuning hyperparameter optimization indicates the parameters with the best performance on the verification set, such as the number of trees in the random forest model, the learning rate in the neural network, the number of iterations, the number of neural network layers, and the number of neurons. The selection and optimization of these hyperparameters are key to the successful implementation of machine learning algorithms. Common hyperparameter optimization approaches include grid search, Bayesian optimization, and gradient elevators [72–74]. The grid search method is a kind of super search algorithm. It can obtain a set of possible values for each hyperparameter to be adjusted, then evaluate the prediction performance of each combination and return the choice of the optimal prediction effect.

Fourthly, model validation and testing indicate that the model performance is validated, along with its testing and evaluation to prevent the model from overfitting or underfitting. Common model performance evaluation indicators include the accuracy rate, correlation coefficient, average absolute percentage error, and root mean square error. For example, the machine learning algorithm used to assist fluid identification in the reactor can predict the offline data and analyze the online unseen data, such as drag force, solid phase stress, and interphase heat transfer [75]. Of course, the coverage and data quality of the data set in the training and learning process also directly determine the later generalizability of the machine learning application.

Based on the above analysis of the flow pattern recognition process in microchannels, this work reviews and comments on the current status of the combination of image and machine learning techniques for flow pattern and heat transfer recognition in microchannels. The image features combined with machine learning algorithms are applied to identify boiling flow patterns to obtain bubble dynamic behavior and flow pattern evolution rules. Besides this, the relationship between flow pattern evolution and BHT is established, and the mechanism of BHT is revealed.

3.2. Application of Machine Learning for Flow Pattern Recognition

3.2.1. Application of Machine Learning to Flow Pattern Image Segmentation and Recognition in Microchannels

Identifying fluid flow patterns in microchannels is mainly performed via feature extraction and classification. The quality of the extracted image features and the classification strategy of the classifier directly determine the classification recognition accuracy and reflect the characteristics of various flow patterns intuitively. Moreover, using image features with differentiation can help to improve the classification accuracy of the classifiers [76].

Figure 6 illustrates the process of image processing and feature extraction for the gas–liquid two-phase fluid in the microchannel.

According to Figure 6, the unprocessed image data cannot be directly used to analyze the flow parameters in the microchannel. Pre-processing processes such as image cropping, noise reduction, contrast enhancement, filtering, and labeling are required to improve the quality of the data set for subsequent image feature extraction and classification recognition. First of all, since the images taken by the high-speed camera include other experimental devices, it is necessary to crop out the parts of the images that are not relevant to the flow pattern. Secondly, some of the flow patterns of the cropped microchannel images are not clearly characterized or have considerable white light noise, which necessitates further noise reduction processing. For example, noise exists in the flow pattern image due to the impurities in the experimental pipeline, the non-uniform light source distribution, and experimental setup jitter. They can be reduced by the Gaussian filtering technique, contrast stretching technique, and Laplace high-pass filtering technique [77–79]. Finally, the features of the fluid image are extracted through the gray histogram and the gradient direction histogram.

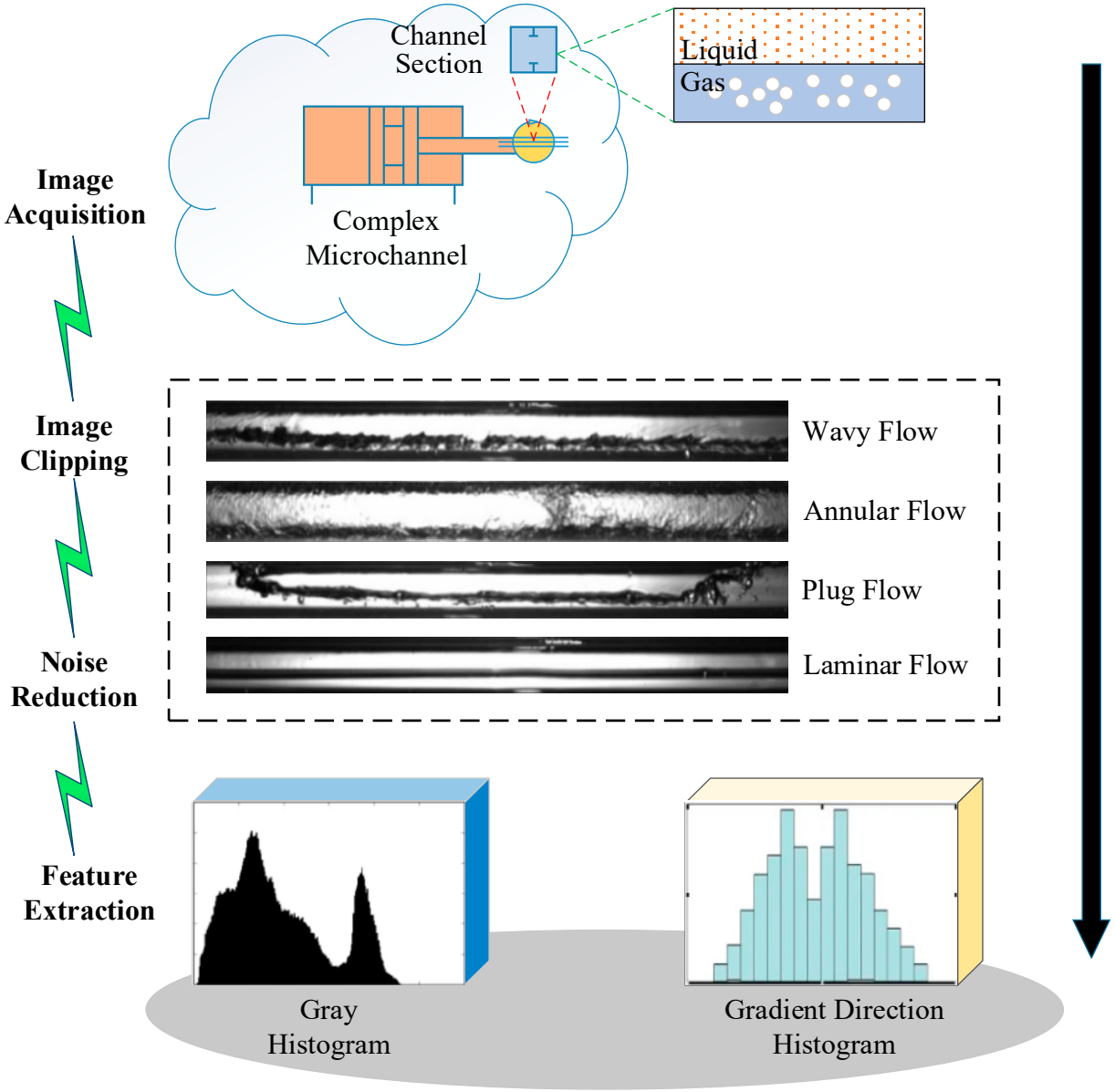

Figure 6. Flow chart of flow pattern image pre-processing and feature extraction in microchannels.

The machine learning algorithm can perform semi-supervised or unsupervised learning on the information in the image data. Therefore, it can autonomously extract the flow image features in the microchannel. As such, many scholars have introduced machine learning to the flow pattern recognition of fluid images. Jakob et al. [80] constructed a large fluid flow dataset and applied it to deep learning (DL) problems in scientific visualization. Finally, a deep convolutional neural network (CNN) was trained using the constructed fluid data set, which significantly improved the recognition accuracy of fluid images and achieved accurate flow pattern analysis. Zhu et al. [81] comprehensively surveyed, explored, analyzed, and discussed key advances from recent years in machine learning applied to fluid mechanics, thermal energy and weight transfer, and response in single-phase and multiphase fluid systems from various perspectives. The authors found that machine learning has shown significant advantages in image reconstruction, state recognition, essential coefficient forecasting, multiphase flow, and transportation sectors. In this way, machine learning and data science can promote the subsequent progress of multiphase flow and reactors. Kim and Park [82] developed a DL-based tool for automatic bubble detection and mask extraction with delayed overfitting using a limited amount of data. The final detection of different bubble streams proved that the model could detect more than 95% of the bubbles with a two-fold higher processing speed than traditional methods. Shen et al. [83] developed an automatic liquid–liquid two-phase flow pattern recognition platform, constructed a CNN with specialist abilities, and combined it with an automatic pumping system and an online high-speed video surveillance system, establishing a high-throughput experimental platform for microchannels. The authors investigated the influence of essential elements such as flow velocity, stickiness, and interface tension, and obtained different flow regimes. Finally, a generalized liquid–liquid two-phase flow pattern map was drawn, providing a basis for understanding complex flow mechanics and patterns. Babanezhad et al. [84] used an adaptive neuro-fuzzy inference system (ANFIS) for flow pattern recognition in 3D cavities. They proved that this predictive method could reduce computation time for fluid visualization in the 3D domain. At the same time, the ANFIS method was very successful in fluid flow pattern recognition compared with the genetic algorithm fuzzy inference system. Yao et al. [85] combined liquid-phase transmission electron microscopy imaging with a customized analysis framework based on the machine learning model, the U-Net neural network, to segment images of a nanoscopic nature. The results indicate that the U-Net combination model showed a superior ability to predict nanoparticle position and shape boundaries from highly noisy and fluctuating backgrounds compared to popular image segmentation methods. It also established a high-throughput and statistically significant way to gain insight into the nanoscale dynamics of synthetic biological nanomaterials. Brunton et al. [86] reported that machine learning had become a critical supplement to the existing experimental, computational, and theoretical aspects of fluid dynamics. The combination of the machine learning and data-driven (D-D) techniques was promising in the field of fluid dynamics.

In summary, machine learning can recognize the low-resolution and strong noise data of flow pattern images, which are robust. Therefore, the combination of image and machine learning technology provides a new approach to intelligent flow pattern recognition in complex structural microchannels. Figure 7 reveals the process of combining image and machine learning technologies for flow pattern recognition in microchannels with complex structures.

In conclusion, many scholars have made efforts towards the identification of two-phase flow patterns and states in complex structural microchannels based on machine learning methods. Manjrekar and Dudukovic [87] used optical probes to measure flow field data in a bubble column reactor, and combined these with the data from the literature (70 sets of data points) for D-D model development. The authors found that the two critical parameters in the detection signal, i.e., the bubble time and the characteristic time, contain a wealth of water domain information. This can be used in the D-D system using SVM to identify the corresponding flow patterns under different test conditions.

Mask et al. [88] collected and analyzed more than 8000 sets of gas–liquid two-phase flow data and studied the gas–liquid flow characteristics. The results show that the flow pattern was mainly affected by parameters such as the fluid properties (including gas–liquid phase density and viscosity), the in-situ flow velocity of liquid and gas, flow channel geometry, and mechanical properties. At the same time, the authors proposed three dimensional variables with specific physical meanings through the dimensional analysis method to reduce the number of parameters, which were taken as the input variables of machine learning. Experiments have demonstrated that a magnitude of one variable significantly improved the prediction accuracy of machine learning. Liu and Bai [89] used a high-speed camera to acquire flow images in an air–water vortex tube. The authors used a self-organizing neural network model to study the flow characteristics under gas–liquid spiral annular flow after extracting the gas–liquid phase content. They also gave a generalized cyclonic flow diagram for identifying cyclonic flow patterns under different operating conditions, such as cyclonic bubbly flow, intermittent cyclonic flow, and cyclonic annular flow. Zhang et al. [90] presented two new parameters, i.e., maximum velocity ratio and maximum velocity difference ratio, to identify clogged and attenuated slug flow. They also utilized two classification algorithms based on Long and Short-Term Memory and CNN to realize fast-response recognition of the transient flow. The results show that the real-time recognition accuracy of the flow pattern could reach 93.1%, and the transient flow pattern recognition under slug flow could be realized with an accuracy of 94% based on the CNN. Pishnamazi et al. [91] compared the artificial intelligence (AI) results of a combined neural network and fuzzy logic approach to an ant colony and fuzzy logic approach. The authors verified that the neural network and fuzzy logic combination method had high potential utility in flow pattern recognition, while the ant colony required much more time to predict and train the system. Furthermore, it was evident that using the ANFIS method could predict a perfect match for the flow pattern and fluid velocity distribution. Barjouei et al. [92] predicted the wellhead throttle flow rate based on DL from four variables: throttle size, wellhead pressure, oil-specific gravity, and gas–liquid ratio. They found that the liquid flow rate was often nonlinearly related to these variables. Besides this, using different reservoir conditions for prediction were conducive to the application of machine learning algorithms in thermodynamics. Kadish et al. [93] used computer vision technology and DL to train the CNN and deep long short-term memory (LSTM) network. CNN was used for individual frame classification and image feature extraction. The deep LSTM network was utilized to collect the timing data in the image characteristic set sequence and implement a terminal categorization of the steam mass or fluid condition. This new two-phase flow achieved a precise assortment of the fluid status and steam content in practical applications of CO_2 two-phase flow in vertical pipes. In addition, the authors used automatically chosen picture characteristics from the CNN framework in three different tests: fluid image categorization, fluid condition categorization and vapor quality forecast. They provided a viable alternative to the manual extraction of image features for image-based flow studies.

The research above suggests that machine learning for the transformation and identification of the flow regimes is mainly concentrated in adiabatic gas–liquid two-phase flow. Research on non-gas–liquid two-phase systems needs to be strengthened. In addition, most approaches are aimed at normal temperature and pressure systems, but research on systems with high temperatures and high pressures is relatively rare. Of course, hyperthermal and high-pressure systems often have high requirements for the manufacture of test and measurement equipment, and involve more difficult measurement than regular-temperature systems.

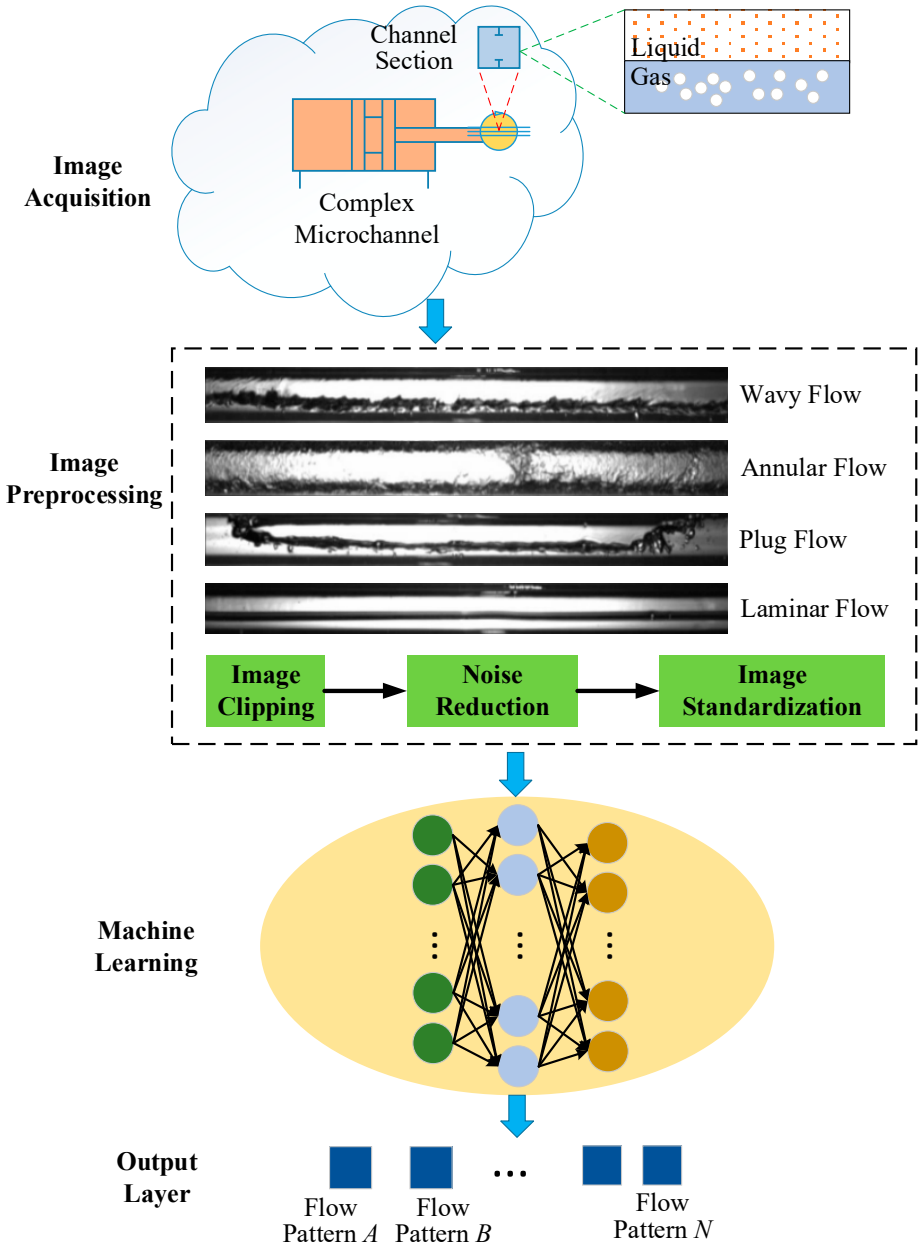

Figure 7. Flow pattern recognition in complex structural microchannels by combining image and machine learning techniques.

3.2.2. Application of Machine Learning for Flow Pattern Identification and Parameter Prediction in Microchannels

Usually, the conventional identification of fluid flow patterns in microchannels primarily analyzes the collected flow pattern data offline. It is challenging to obtain real-time data on transient flow. The application of machine learning can realize real-time predictions based on the instantaneous data in the microchannel [94,95]. Many scholars have predicted the fluid flow patterns using machine learning. Loyola-Fuentes et al. [96] collected experimental data for two operating liquids (ethanol and FC-72) in a pulsating heat pipe at different gravity and power input levels for training three different classification algorithms (i.e., K-nearest neighbor (KNN), random forest, and multi-layer perceptron). They used the experimental results to pre-label the data by visual classification. Eventually, they compared the classification accuracies using confusion matrix and accuracy scores. The results show that the three classification algorithms can accurately indicate the flow transition boundary between segment plug/plug and annular flow, which helps to reduce

the uncertainty in flow classification and improve flow prediction. Zhang et al. [97] used machine learning to build an algorithm that automatically identifies, judges, and predicts flow patterns and droplet characteristics, thereby transforming empirical judgment into an intelligent process. Simulations verified that the support vector machine (SVM) and back propagation neural network (BPNN) algorithms can successfully classify and predict different flow patterns and droplet characteristics (length and frequency). Moreover, the comparison with the original parametric system proves that the dimensionless number system has a better prediction ability. The machine learning algorithm of dimensionless numbers for the flow pattern prediction of fluid can significantly reduce the dimension and calculation requirements of the system, and maintain the information of the original parameters. Ooi et al. [98] used the conductivity probe signal as input data, applied machine learning technology to identify the boiling flow pattern in the vertical ring channel, and proposed a two-step method to identify local and global flow states using self-organizing map (SOM). The global flow pattern identified by SOM was used as a reference, and the supervised SVM and KNN algorithms with the features extracted by the conductivity probe were trained. The model used the global flow pattern identified by SOM as the reference and the flow pattern feature dataset as the input; the accuracy of the flow pattern classification exceeded 90%.

Arief et al. [99] reported that distributed optical fiber sensing plays a critical part in the real-time monitoring of multiphase fluid flow in industrial flow measurement. They analyzed the D-D machine learning algorithms, such as SVM, CNN, and Integrated Kalman Filter algorithms. The review helped terminal users to build robust, dependable, and rigid answers, paving the way for the intellectual development of the predictive recognition of flow regimes in thermodynamics. Han and Kwon [100] proposed a selective surrogate architecture based on a D-D DL model. They applied a deep neural network (DNN) via the multilayer perceptron as the dependent variable to predict cumulative gas production to analyze well completion, hydrofracture, and productivity data. The results indicate that the DNN model could predict the fluid state well, employing a principal component with an accumulative contribution rate of 85%. Besides this, the optimal forecast accuracy of the model's average absolute percentage error increased to 0.2~9.1%, providing helpful guidance for economical diagnosis and potential exploitation projects at nearby reservoirs. Dehghan Manshadi et al. [101] used an LSTM algorithm for the predictive modeling of time-series prediction accuracy to simulate fluid–solid interactions. The authors found that a comparative analysis between the simulated and predicted results indicated that the LSTM method was suitable for modeling. In addition, the LSTM method significantly reduced the computation time, showed the mathematical relationship of the output power, and helped extend it to a wider range of parameters.

In general, machine learning can not only be used to identify flow patterns, but can also accurately predict flow patterns according to the various operating parameters, and design geometry parameters. At the same time, it plays a vital role in understanding the heat transfer characteristics in microchannels and the stable operation of electronic components due to the equal importance of heat and mass transfer.

3.2.3. Application of SVM for Flow Pattern and Texture Feature Recognition in Microchannels

SVM is a new machine algorithm based on statistical learning theory and the structural risk minimization principle. The algorithm is able to find the best balance between model sophistication and learning capability to acquire the optimal generalization ability based on restricted specimen information [102,103]. SVM for feature recognition in flow regimes has been investigated by numerous scholars.

Roshani et al. [104] proposed a smart non-destructive technique based on the combination of gamma radiation attenuation and AI to determine the flow regime type and gas volume percentage in two-phase flow. At the same time, they employed SVM to identify the state of the fluid, and adopted the multi-layer perceptron of the Levenberg–Marquardt

algorithm to predict the porosity of the fluid. The results show that the system could identify the annular region and measure the void fraction independent of the scale layer thickness of the oil pipeline. Shanthi et al. [105] used SVM and neural network methods to extract features of gas–liquid two-phase flow patterns in vertical microchannels, and identify flow patterns. A high-speed camera was used to capture the flow images. After image preprocessing, texture features, such as entropy, uniformity, contrast, correlation and energy of the image, were extracted. The extracted texture features were used as input for the pattern recognition of segmental slug flow by combining a neural network and SVM classifier. The experimental setup captured four typical flow patterns, such as bubbly flow, segmental slug flow, stratified flow and annular flow. Compared with the neural network classifier, the SVM achieved an accuracy of 98% in classifying the segment plug flow. The results show that the texture method combined with the SVM classifier was feasible, and could be applied to the classification of two-phase flows with high accuracy. Masood and Farooq [106] evaluated image features and SVM classifiers for image recognition on a dataset with view variations in high-scene depth videos. The algorithmic recognition technique achieved remarkable accuracy across all appearances and views. Rasel et al. [107] found that Electrical Capacitance Volume Tomography (ECVT) could monitor multiple flow conditions. The authors reconstructed real-time 3D images from capacitance measurements using a set of electrode plates placed around a process column surrounding a sensing flow system. The results show that ECVTs were non-invasive, allowing the measurement of variations in mutual capacitance with all possible combinations of board pairs. Moreover, the SVM algorithm could realize the robust monitoring of multiphase flow, especially water multiphase flow.

Generally speaking, SVM technology can take advantage of small sample training in the complex flow pattern recognition of microchannel electronic components. Meanwhile, the SVM algorithm provides a description of the complexity independent of the dimension of the problem, thus avoiding the problems of the difficult convergence, complex calculation, and difficult interpretation of results when dealing with high-dimensional data [108,109]. Therefore, the SVM algorithm can construct a linear decision boundary in the high-dimensional feature space to recognize the flow patterns in the microchannel [110]. The upper bound of the expected risk of SVM can be expressed as Equation (1).

$$E[\Pr(error)] \leq E(N_a)/(N_x - 1) \quad (1)$$

In Equation (1), N_a refers to the number of SVMs, and N_x represents the number of training vectors. It can be seen that reducing the number of support vectors can improve the generalization ability of SVM and improve the accuracy of flow pattern recognition in microchannels with complex structures.

3.3. Application of Machine Learning for Boiling Flow Pattern Recognition in Microchannels

Boiling is considered to be the most efficient thermal management method in nature. It cools the heating surface by the transport of advection resulting from bubbles. The core of BHT is the formation of bubbles [111–113]. Linking the physics of boiling to bubble dynamics kinetics is an essential and daunting challenge. Suh et al. [114] introduced a D-D learning architecture that associates the qualified imaging of kinetic bubbles with related boiling curves. The frontier DL models were applied, including the CNN and object inspection methods for the automatical extraction of stratified and physics-based characteristics. The authors interpreted the physical mechanism of boiling by training these features. The model described the way bubbles nucleate, aggregate, and detach under seething conditions, resulting in an average error of 6% in in situ seething profile estimation. Therefore, this architecture could provide a learning-based automated method substituting the traditional BHT metrology. Zhu et al. [115] proposed and trained an artificial neural network (ANN) model based on machine learning to predict the HTP of flow boiling and condensation. They found that the mean absolute relative deviation of the ANN model for boiling and condensation was 11.41% and 6.06%, respectively. The test results show

that a reasonable ANN model could be constructed using the most critical parameters instead of all available parameters. Moreover, the ANN model could provide a reference for future two-phase flow research, and be used for practical design, which will benefit advanced thermal management systems. Rokoni et al. [116] used principal component analysis (PCA) to retrieve novel material descriptive subsets of BHT from images of pool boiling experiments. The results show that dominant frequencies and amplitudes could be used as novel material descriptive subsets to differentiate various states. Experimental results demonstrate that the main frequency of the first principal component grows with the growth of heat flux in the dissociated bubble region until it attains a crest value. It then falls off with the growth of heat flux in the bubble intervention and merging region. The extracted dominant frequencies and amplitudes were further qualitatively compared with the bubble counts and sizes collected from a supervised DL algorithm. The method was found to have strong robustness over multiple data sets and heating surfaces. In addition, the bidirectional LSTM (BiLSTM) neural network algorithm was employed to evaluate the upcoming variations in the principal component from the temporal sequences to predict the future boiling state, so as to alleviate the boiling crisis and assess the bubble dynamics. The authors found that the PCA-based BiLSTM model precisely predicts low-level bubble pictures, apparently outperforming the convolutional LSTM network in forecast precision. He et al. [117] collected a comprehensive dataset of 484 subcooled flow boiling bubble departure frequencies from 10 data sources, and used a machine learning-based approach to predict the bubble departure frequencies in subcooled flow boiling. A unified dataset of subcooled flow boiling bubble departure frequencies with four workloads was established, and nine machine learning-based regression models were discussed in detail, including: linear regression, decision tree, Random Forest, AdaBoost, Gradient Boosting, XGBoost, SVM, KNN and Bagging. The input parameters (including geometric parameters and dimensionless parameters) were compared to obtain a suitable method. Among them, the prediction performance of the XGBoost model continued to perform well. The machine learning-based approach provides a reliable tool for bubble departure frequency prediction.

Zajec et al. [118] explored the effect of heat flux variation on the boiling flow pattern under approximately constant inlet flow conditions (fixed mass flux and fluid inlet temperature) of the operational liquid. The boiling process of the supercooled flow was recorded using a high-speed camera. Meanwhile, the images were analyzed using a neural network algorithm to determine the bubble size distribution and its variation with heat flux. Finally, the authors employed the mechanism of the image combined with a neural network to identify the boiling mechanism. Galicia et al. [119] conducted an experimental study on the use of highly sintered fibers attached to the surface to enhance supercooled flow boiling. A bare surface and four porous thicknesses were compared at three different mass fluxes and inlet subcooling temperatures. The results show that the porous body could increase the heat flux and reduce the superheated temperature of the wall. However, high porous thicknesses reduced heat flux compared to bare surfaces. Additionally, it was found that bubble size and formation are generally small at high inlet subcooling temperatures by recording bubble formation and patterned flow with a high-speed camera. The increased heat flux and reduced wall superheating were attributed to the increased nucleation sites, increased heating surface area, water supply capacity, and vapor trapping capacity through the porous body.

In summary, machine learning has significant advantages in flow pattern recognition. Using flow pattern image features combined with machine learning algorithms to identify boiling flow patterns can enable the prediction of bubble changes and highlight the evolution mechanism of microchannel boiling flow patterns.

4. Discussion and Outlook

The heat dissipation of micro-devices with high heat flux has become an urgent problem that must be solved. Microchannel BHT is one of the most effective methods for removing high heat loads from micro-devices. In the process of microchannel BHT, the

flow pattern changes constantly, and different flow patterns correspond to different heat transfer mechanisms. Therefore, accurate identification of the flow pattern is an effective way to understand the flow boiling in microchannels.

For microchannels with complex structures, the flow patterns are more complex and difficult to measure due to the randomness and chaotic characteristics of their flow pattern evolution. The discriminative accuracy of visual analysis using high-speed cameras is not enough, and the observation is difficult. On the other hand, the rapid development of computer vision technology provides a new way to extract quantitative information about the bubble behavior and flow pattern evolution. With the help of computer vision technology, image processing is performed to improve the image quality, and the accuracy of the flow pattern identification during flow boiling process provides an important reference for establishing the bubble dynamic model and revealing the interrelationship between flow and heat transfer.

As a machine learning algorithms, SVM is a recognition method based on the flow pattern. It has low dependence on sample data, strong generalizability, short training time, and a high recognition rate. SVM can effectively recognize the flow patterns of gas–liquid two-phase flow in horizontal pipes. At the same time, SVM can obtain similar results for each training after the initial parameters are given. In particular, when the number of samples is small, a better recognition effect is achieved than with the neural network, and it is more suitable for flow pattern online recognition. However, it is currently mostly eligible for the intelligent recognition of flow pattern images of sparse bubbles (bubbles do not overlap) in microchannels. A suitable segmentation algorithm is essential for bubble images with overlapping.

It is necessary to analyze the research status of applying machine learning to the identification of boiling flow patterns and evolution rules. Besides this, the changing trend of the two-phase velocity ratio in the process of flow pattern transition in the experiment should be explained from the perspective of the mechanism. Then, the criterion of flow pattern transformation should be established based on this mechanism to precisely reveal the mechanism of flow pattern evolution. The final criterion is expressed in the form of a critical cavity fraction, which is an instantaneous change. However, the essence of the criterion is an extremum relationship—a gradual process rather than a sudden evariation. The process can be matched with the bubble size to select the appropriate flow transition region, reflecting the nature of the flow transition. In addition, the flow pattern transition criterion can be used to predict the flow pattern transition under different conditions, such as different working conditions and channel sizes, with high accuracy. This is also the direction of follow-up research on BHT mechanisms in complex microchannels.

5. Conclusions

Microchannel BHT is one of the most effective methods for removing high heat loads from micro-devices. During the boiling process inside the microchannel, the flow pattern changes continuously due to the variation of vapor quality along the flow direction, and different flow patterns correspond to different heat transfer mechanisms. This paper first summarizes a high-speed camera visualization study of flow boiling in microchannels, including some novel microchannel structures and different wettability surfaces, as well as the flow pattern identification in microchannels using computer vision techniques. It attempts to elucidate the mechanisms of enhanced BHT by microchannel structures through the accurate identification of the flow pattern evolution during boiling. The research on the application of machine learning methods for flow pattern recognition in microchannels is reviewed, reflecting the advantages of the combination of flow pattern images and machine learning techniques applied to flow pattern and heat transfer recognition in microchannels. Many factors influence flow pattern identification, including the diversity of flow patterns and the limitations of detection methods. The flow pattern evolution in microchannels with complex geometric structures, in particular, exhibits random and chaotic characteristics in both time and space, making flow pattern identification more difficult. As a result,

determining the influence of the flow pattern evolution on BHT mechanisms is difficult. Computer vision technology and machine learning methods provide a new method for microchannel flow pattern identification. Computer vision techniques extract quantitative information on bubble behavior and flow pattern evolution, which can provide important references for establishing bubble dynamic models and revealing the interrelationship between the flow and heat transfer. Computer vision and machine learning can be used for the real-time monitoring of the flow field and temperature field to predict boiling crises and flow instability in micro heat sinks.

Author Contributions: Conceptualization, B.Y.; methodology, M.L. and X.Z.; visualization, Y.L.; investigation, B.W., X.Z., M.L. and Z.L.; writing—original draft, X.Z. and M.L.; writing—review and editing Y.L. and F.W.; supervision, B.Y.; project administration, M.L. and B.Y. All authors have read and agreed to the published version of the manuscript.

Funding: This research was funded by the National Natural Science Foundation of China (No. 52108467) and the National Natural Science Foundation of China (No. 52278119).

Data Availability Statement: Data available on request due to restrictions e.g., privacy or ethical.

Conflicts of Interest: The authors declare no conflict of interest.

Abbreviations

AI	Artificial intelligence
ANFIS	Adaptive neuro-fuzzy inference system
ANN	Artificial neural network
AR	Aspect ratio
BCF	Bidirectional counter-flow
BHT	Boiling heat transfer
BPNN	Back Propagation Neural Network
CBT	Convective boiling heat transfer
CCD	Charge-coupled device
CHF	Critical heat flux
CMC	Carboxymethyl cellulose
CNN	Convolutional neural network
D-D	Data-driven
DNN	Deep neural network
DL	Deep learning
ECVT	Electrical Capacitance Volume Tomography
GA-BP	Genetic Algorithm optimized Back Propagation
HPI	Hydrophilic
IM	Interconnected microchannels
IR	Infrared
KNN	K-nearest neighbor
LFDM	Laser confocal displacement meter
LSTM	Long short-term memory
ONB	Start of nucleate boiling
ORPFM	Open-ring pin fin microchannels
PCA	Principal component analysis
PM	Plain-wall microchannel
SHPI	Super hydrophilic
SHPO	Super hydrophobic
SOM	Self-organizing map
SVM	Support vector machine
UPF	Unidirectional parallel flow

References

1. He, Z.; Yan, Y.; Zhang, Z. Thermal management and temperature uniformity enhancement of electronic devices by micro heat sinks: A review. *Energy* **2020**, *216*, 119223. [CrossRef]
2. Ding, B.; Zhang, Z.-H.; Gong, L.; Xu, M.-H.; Huang, Z.-Q. A novel thermal management scheme for 3D-IC chips with multi-cores and high power density. *Appl. Therm. Eng.* **2019**, *168*, 114832. [CrossRef]
3. Karayiannis, T.; Mahmoud, M. Flow boiling in microchannels: Fundamentals and applications. *Appl. Therm. Eng.* **2017**, *115*, 1372–1397. [CrossRef]
4. Murshed, S.S.; De Castro, C.N. A critical review of traditional and emerging techniques and fluids for electronics cooling. *Renew. Sust. Energ. Rev.* **2017**, *78*, 821–833. [CrossRef]
5. Sardeshpande, M.V.; Ranade, V.V. Two-phase flow boiling in small channels: A brief review. *Sadhana* **2013**, *38*, 1083–1126. [CrossRef]
6. Kandlikar, S.G. Fundamental issues related to flow boiling in minichannels and microchannels. *Exp. Therm. Fluid Sci.* **2002**, *26*, 389–407. [CrossRef]
7. Wang, Y.; Wang, Z.G. An overview of liquid–vapor phase change, flow and heat transfer in mini-and micro-channels. *Int. J. Therm. Sci.* **2014**, *86*, 227–245. [CrossRef]
8. Choi, C.; Kim, M. Flow pattern based correlations of two-phase pressure drop in rectangular microchannels. *Int. J. Heat Fluid Flow* **2011**, *32*, 1199–1207. [CrossRef]
9. Krishnamurthy, S.; Peles, Y. Flow Boiling Heat Transfer on Micro Pin Fins Entrenched in a Microchannel. *J. Heat Transf.* **2010**, *132*, 041007. [CrossRef]
10. Kadam, S.T.; Kumar, R. Twenty first century cooling solution: Microchannel heat sinks. *Int. J. Therm. Sci.* **2014**, *85*, 73–92. [CrossRef]
11. Zhang, D.; Xu, H.; Chen, Y.; Wang, L.; Qu, J.; Wu, M.; Zhou, Z. Boiling Heat Transfer Performance of Parallel Porous Microchannels. *Energies* **2020**, *13*, 2970. [CrossRef]
12. Kim, S.M.; Mudawar, I. Universal approach to predicting saturated flow boiling heat transfer in mini/micro-channels–Part II. Two-phase heat transfer coefficient. *Int. J. Heat Mass Transf.* **2013**, *64*, 1239–1256. [CrossRef]
13. Chen, Y.; Wu, Z.; Zhao, B.; Fan, C.; Shi, S. Weed and Corn Seedling Detection in Field Based on Multi Feature Fusion and Support Vector Machine. *Sensors* **2020**, *21*, 212. [CrossRef]
14. Win, K.; Maneerat, N.; Hamamoto, K.; Sreng, S. Hybrid Learning of Hand-Crafted and Deep-Activated Features Using Particle Swarm Optimization and Optimized Support Vector Machine for Tuberculosis Screening. *Appl. Sci.* **2020**, *10*, 5749. [CrossRef]
15. Daneshfaraz, R.; Bagherzadeh, M.; Esmaeeli, R.; Norouzi, R.; Abraham, J. Study of the performance of support vector machine for predicting vertical drop hydraulic parameters in the presence of dual horizontal screens. *Water Supply* **2020**, *21*, 217–231. [CrossRef]
16. Zhu, L.; Spachos, P.; Pensini, E.; Plataniotis, K.N. Deep learning and machine vision for food processing: A survey. *Curr. Res. Food Sci.* **2021**, *4*, 233–249. [CrossRef]
17. Li, Z.; Ma, J. Discussing street tree planning based on pedestrian volume using machine learning and computer vision. *Build. Environ.* **2022**, *219*, 109178. [CrossRef]
18. Li, W.; Zhang, L.; Wu, C.; Cui, Z.; Niu, C. A new lightweight deep neural network for surface scratch detection. *Int. J. Adv. Manuf. Technol.* **2022**, *123*, 1999–2015. [CrossRef]
19. Huang, H.; Pan, L.-M.; Yan, R.-G. Flow characteristics and instability analysis of pressure drop in parallel multiple microchannels. *Appl. Therm. Eng.* **2018**, *142*, 184–193. [CrossRef]
20. Yu, D.; Hu, X.; Guo, C.; Xie, N.; Tang, D. Visualization of microbubble dynamic behaviors in open rectangular microgrooves heat sinks under saturated boiling condition. *Appl. Therm. Eng.* **2015**, *80*, 424–435. [CrossRef]
21. Qu, W.; Mudawar, I. Measurement and prediction of pressure drop in two-phase micro-channel heat sinks. *Int. J. Heat Mass Transf.* **2003**, *46*, 2737–2753. [CrossRef]
22. Shen, B.; Yan, H.; Sunden, B.; Xue, H.; Xie, G. Forced convection and heat transfer of water-cooled microchannel heat sinks with various structured metal foams. *Int. J. Heat Mass Transf.* **2017**, *113*, 1043–1053. [CrossRef]
23. Suo, M.; Griffith, P. Two-Phase Flow in Capillary Tubes. *J. Basic Eng.* **1964**, *86*, 576–582. [CrossRef]
24. Thome, J.; Bar-Cohen, A.; Revellin, R.; Zun, I. Unified mechanistic multiscale mapping of two-phase flow patterns in microchannels. *Exp. Therm. Fluid Sci.* **2013**, *44*, 1–22. [CrossRef]
25. Charnay, R.; Revellin, R.; Bonjour, J. Flow boiling heat transfer in minichannels at high saturation temperatures: Part I–Experimental investigation and analysis of the heat transfer mechanisms. *Int. J. Heat Mass Transf.* **2015**, *87*, 636–652. [CrossRef]
26. Mahmoud, M.M.; Karayiannis, T.G. Flow pattern transition models and correlations for flow boiling in mini-tubes. *Exp. Therm. Fluid Sci.* **2016**, *70*, 270–282. [CrossRef]
27. Ong, C.; Thome, J. Macro-to-microchannel transition in two-phase flow: Part 2—Flow boiling heat transfer and critical heat flux. *Exp. Therm. Fluid Sci.* **2011**, *35*, 873–886. [CrossRef]
28. Li, J.; Zhu, Z.; Zhao, L.; Peng, H. Experimental investigation of the heat transfer and flow characteristics of microchannels with microribs. *Int. J. Heat Mass Transf.* **2019**, *143*, 118482. [CrossRef]
29. Deng, D.; Zeng, L.; Sun, W.; Pi, G.; Yang, Y. Experimental study of flow boiling performance of open-ring pin fin microchannels. *Int. J. Heat Mass Transf.* **2020**, *167*, 120829. [CrossRef]

30. Lyu, Z.; Xu, J.; Yu, X.; Jin, W.; Zhang, W. Wavelet decomposition method decoupled boiling/evaporation oscillation mechanisms over two to three timescales: A study for a microchannel with pin fin structure. *Int. J. Multiph. Flow* **2015**, *72*, 53–72. [CrossRef]
31. Das, S.; Subudhi, S. A review on different methodologies to study thermal comfort. *Int. J. Environ. Sci. Technol.* **2021**, *19*, 2155–2171. [CrossRef]
32. Ma, D.; Xia, G.; Wang, W.; Jia, Y.; Yang, Y. Study on thermal performance of microchannel heat sinks with periodic jetting and throttling structures in sidewalls. *Appl. Therm. Eng.* **2019**, *158*, 113764. [CrossRef]
33. Zhang, P.; Wang, T.; Jiang, Y.; Guo, C. Measurement of transient liquid film and its effect on flow boiling heat transfer in non-circular microchannels. *Int. J. Therm. Sci.* **2023**, *184*, 108004. [CrossRef]
34. Lin, P.; Fu, B.; Pan, C. Critical heat flux on flow boiling of methanol–water mixtures in a diverging microchannel with artificial cavities. *Int. J. Heat Mass Transf.* **2011**, *54*, 3156–3166. [CrossRef]
35. Zhou, K.; Zhu, H.; Li, W.; Li, J.; Sheng, K.; Shao, S.; Li, H.; Tao, Z. Heat Transfer Characteristics and Flow Pattern Visualization for Flow Boiling in a Vertical Narrow Microchannel. *J. Electron. Packag.* **2019**, *141*, 031006. [CrossRef]
36. Liao, W.-R.; Chien, L.-H.; Ghalambaz, M.; Yan, W.-M. Experimental study of boiling heat transfer in a microchannel with nucleated-shape columnar micro-pin-fins. *Int. Commun. Heat Mass Transf.* **2019**, *108*, 104277. [CrossRef]
37. Yang, Q.; Shu, B.; Wang, J.; Guo, Y. Experimental investigation on flow boiling heat transfer and flow patterns in a single micro-channel with large mass velocity. *Exp. Therm. Fluid Sci.* **2018**, *91*, 283–291. [CrossRef]
38. Feng, K.; Zhang, H. Pressure drop and flow pattern of gas-non-Newtonian fluid two-phase flow in a square microchannel. *Chem. Eng. Res. Des.* **2021**, *173*, 158–169. [CrossRef]
39. Cheng, X.; Wu, H. Enhanced flow boiling performance in high-aspect-ratio groove-wall microchannels. *Int. J. Heat Mass Transf.* **2020**, *164*, 120468. [CrossRef]
40. Cheng, X.; Wu, H. Improved flow boiling performance in high-aspect-ratio interconnected microchannels. *Int. J. Heat Mass Transf.* **2021**, *165*, 120627. [CrossRef]
41. Li, Y.; Xia, G.; Ma, D.; Yang, J.; Li, W. Experimental investigation of flow boiling characteristics in microchannel with triangular cavities and rectangular fins. *Int. J. Heat Mass Transf.* **2020**, *148*, 119036. [CrossRef]
42. Wu, H.; Cheng, P. Visualization and measurements of periodic boiling in silicon microchannels. *Int. J. Heat Mass Transf.* **2003**, *46*, 2603–2614. [CrossRef]
43. Alam, T.; Lee, P.S.; Yap, C.R.; Jin, L. A comparative study of flow boiling heat transfer and pressure drop characteristics in microgap and microchannel heat sink and an evaluation of microgap heat sink for hotspot mitigation. *Int. J. Heat Mass Transf.* **2013**, *58*, 335–347. [CrossRef]
44. Alam, T.; Li, W.; Yang, F.; Chang, W.; Li, J.; Wang, Z.; Khan, J.; Li, C. Force analysis and bubble dynamics during flow boiling in silicon nanowire microchannels. *Int. J. Heat Mass Transf.* **2016**, *101*, 915–926. [CrossRef]
45. Prajapati, Y.K.; Pathak, M.; Khan, M.K. A comparative study of flow boiling heat transfer in three different configurations of microchannels. *Int. J. Heat Mass Transf.* **2015**, *85*, 711–722. [CrossRef]
46. Markal, B.; Kul, B.; Avci, M.; Varol, R. Effect of gradually expanding flow passages on flow boiling of micro pin fin heat sinks. *Int. J. Heat Mass Transf.* **2022**, *197*, 123355. [CrossRef]
47. Yin, L.; Jiang, P.; Xu, R.; Wang, W.; Jia, L. Visualization of flow patterns and bubble behavior during flow boiling in open microchannels. *Int. Commun. Heat Mass Transf.* **2017**, *85*, 131–138. [CrossRef]
48. Li, Y.; Wu, H. Experiment investigation on flow boiling heat transfer in a bidirectional counter-flow microchannel heat sink. *Int. J. Heat Mass Transf.* **2022**, *187*, 122500. [CrossRef]
49. Lee, J.; Devahdhanush, V.; Darges, S.J.; Mudawar, I. Effects of flow loop compressible volume position on system instabilities during flow boiling in micro-channel heat sinks. *Int. J. Heat Mass Transf.* **2022**, *198*, 123394. [CrossRef]
50. Liu, G.; He, C.; Wen, Q.; Wang, Z.; Wang, X.; Shittu, S.; Zhao, X.; Hu, M. Investigation on visualization and heat transfer performance study of the mini-channel flow boiling. *Int. Commun. Heat Mass Transf.* **2022**, *138*, 106360. [CrossRef]
51. Vermaak, M.; Potgieter, J.; Dirker, J.; A Moghimi, M.; Valluri, P.; Sefiane, K.; Meyer, J.P. Experimental and Numerical Investigation of Micro/Mini Channel Flow-Boiling Heat Transfer with Non-Uniform Circumferential Heat Fluxes at Different Rotational Orientations. *Int. J. Heat Mass Transf.* **2020**, *158*, 119948. [CrossRef]
52. Hong, S.; Tang, Y.; Lai, Y.; Wang, S. An experimental investigation on effect of channel configuration in ultra-shallow micro multi-channels flow boiling: Heat transfer enhancement and visualized presentation. *Exp. Therm. Fluid Sci.* **2017**, *83*, 239–247. [CrossRef]
53. Halon, S.; Krolicki, Z.; Revellin, R.; Zajaczkowski, B. Local flow patterns distribution during flow boiling in a micro channel array. *Exp. Therm. Fluid Sci.* **2023**, *141*, 110792. [CrossRef]
54. Hong, S.; Tang, Y.; Dang, C.; Wang, S. Experimental research of the critical geometric parameters on subcooled flow boiling in confined microchannels. *Int. J. Heat Mass Transf.* **2018**, *116*, 73–83. [CrossRef]
55. Zhou, S.; Shu, B.; Yu, Z.; Huang, Y.; Zhang, Y. Experimental Study and Mechanism Analysis of the Flow Boiling and Heat Transfer Characteristics in Microchannels with Different Surface Wettability. *Micromachines* **2021**, *12*, 881. [CrossRef]
56. Zhao, Q.; Qiu, J.; Zhou, J.; Lu, M.; Li, Q.; Chen, X. Visualization study of flow boiling characteristics in open microchannels with different wettability. *Int. J. Heat Mass Transf.* **2021**, *180*, 121808. [CrossRef]
57. Qin, L.; Li, S.; Zhao, X.; Zhang, X. Experimental research on flow boiling characteristics of micro pin-fin arrays with different hydrophobic coatings. *Int. Commun. Heat Mass Transf.* **2021**, *126*, 105456. [CrossRef]

58. Fore, L.; Ibrahim, B.; Beus, S. Visual measurements of droplet size in gas–liquid annular flow. *Int. J. Multiph. Flow* **2002**, *28*, 1895–1910. [CrossRef]
59. Hanafizadeh, P.; Ghanbarzadeh, S.; Saidi, M.H. Visual technique for detection of gas–liquid two-phase flow regime in the airlift pump. *J. Pet. Sci. Eng.* **2011**, *75*, 327–335. [CrossRef]
60. Harrison, S.T.; Stevenson, R.; Cilliers, J.J. Assessing solids concentration homogeneity in Rushton-agitated slurry reactors using electrical resistance tomography (ERT). *Chem. Eng. Sci.* **2012**, *71*, 392–399. [CrossRef]
61. Babaei, R.; Bonakdarpour, B.; Ein-Mozaffari, F. Analysis of gas phase characteristics and mixing performance in an activated sludge bioreactor using electrical resistance tomography. *Chem. Eng. J.* **2015**, *279*, 874–884. [CrossRef]
62. Huang, J.; Xu, J.; Sang, X.; Wang, H.; Wang, H. Quantifying the synergy of bubble swarm patterns and heat transfer performance using computational homology. *Int. J. Heat Mass Transf.* **2014**, *75*, 497–503. [CrossRef]
63. Fei, Y.; Xiao, Q.; Xu, J.; Pan, J.; Wang, S.; Wang, H.; Huang, J. A novel approach for measuring bubbles uniformity and mixing efficiency in a direct contact heat exchanger. *Energy* **2015**, *93*, 2313–2320. [CrossRef]
64. Li, H.; Hrnjak, P. Visualization of R1234yf, R1233zd (E), and R1336mzz (Z) flow in microchannel tube with emphasis on the velocity of vapor plugs. *Heat Mass Transf.* **2022**, *58*, 17. [CrossRef]
65. Liu, T.-L.; Pan, C. Infrared thermography measurement of two-phase boiling flow heat transfer in a microchannel. *Appl. Therm. Eng.* **2016**, *94*, 568–578. [CrossRef]
66. Huang, H.; Thome, J.R. Local measurements and a new flow pattern based model for subcooled and saturated flow boiling heat transfer in multi-microchannel evaporators. *Int. J. Heat Mass Transf.* **2016**, *103*, 701–714. [CrossRef]
67. Korniliou, S.; Mackenzie-Dover, C.; Christy, J.R.; Harmand, S.; Walton, A.J.; Sefiane, K. Two-dimensional heat transfer coefficients with simultaneous flow visualisations during two-phase flow boiling in a PDMS microchannel. *Appl. Therm. Eng.* **2018**, *130*, 624–636. [CrossRef]
68. Liu, Y.; Yao, X.; Gu, Z.; Zhou, Z.; Liu, X.; Chen, X.; Wei, S. Study of the Automatic Recognition of Landslides by Using InSAR Images and the Improved Mask R-CNN Model in the Eastern Tibet Plateau. *Remote Sens.* **2022**, *14*, 3362. [CrossRef]
69. Hughes, M.T.; Kini, G.; Garimella, S. Status, Challenges, and Potential for Machine Learning in Understanding and Applying Heat Transfer Phenomena. *J. Heat Transf.* **2021**, *143*, 120802. [CrossRef]
70. Hachem, E.; Ghraieb, H.; Viquerat, J.; Larcher, A.; Meliga, P. Deep reinforcement learning for the control of conjugate heat transfer. *J. Comput. Phys.* **2021**, *436*, 110317. [CrossRef]
71. Vahedi, S.M.; Aghakhani, S.; Pordanjani, A.H.; Azaiez, J. A comprehensive parametric study on heat transfer optimization of a triangular enclosure subjected to a magnetic field using neural network machine learning. *Eng. Anal. Bound. Elem.* **2022**, *145*, 173–186. [CrossRef]
72. Hawkins, A.J.; Fox, D.B.; Koch, D.L.; Becker, M.W.; Tester, J.W. Predictive inverse model for advective heat transfer in a short-circuited fracture: Dimensional analysis, machine learning, and field demonstration. *Water Res. Res.* **2020**, *56*, e2020WR027065. [CrossRef]
73. Zhou, L.; Garg, D.; Qiu, Y.; Kim, S.-M.; Mudawar, I.; Kharangate, C.R. Machine learning algorithms to predict flow condensation heat transfer coefficient in mini/micro-channel utilizing universal data. *Int. J. Heat Mass Transf.* **2020**, *162*, 120351. [CrossRef]
74. Chen, X.; Lv, H. Intelligent control of nanoparticle synthesis on microfluidic chips with machine learning. *NPG Asia Mater.* **2022**, *14*, 69. [CrossRef]
75. Chen, G. Non-Fourier phonon heat conduction at the microscale and nanoscale. *Nat. Rev. Phys.* **2021**, *3*, 555–569. [CrossRef]
76. Yu, S.; Zhang, L.; Wang, A.; Ni, L. Joint prediction of internal and external temperatures for cylindrical Li-ion batteries. *J. Power Electron.* **2022**, *22*, 1938–1946. [CrossRef]
77. Li, H.; Yu, S.; Yang, W.; Luo, J. Flow Pattern Identification for Gas-Liquid Two-Phase Flow in Minichannel Based on a New Optical Array Sensor. *IEEE Sens. J.* **2021**, *21*, 19334–19340. [CrossRef]
78. Liu, L.; Guo, C.; Xiang, Y.; Tu, Y.; Wang, L.; Xuan, F.-Z. A Semisupervised Learning Framework for Recognition and Classification of Defects in Transient Thermography Detection. *IEEE Trans. Ind. Inform.* **2021**, *18*, 2632–2640. [CrossRef]
79. Moghadasi, H.; Saffari, H. Experimental study of nucleate pool boiling heat transfer improvement utilizing micro/nanoparticles porous coating on copper surfaces. *Int. J. Mech. Sci.* **2021**, *196*, 106270. [CrossRef]
80. Jakob, J.; Gross, M.; Gunther, T. A Fluid Flow Data Set for Machine Learning and its Application to Neural Flow Map Interpolation. *IEEE Trans. Vis. Comput. Graph.* **2020**, *27*, 1279–1289. [CrossRef]
81. Zhu, L.-T.; Chen, X.-Z.; Ouyang, B.; Yan, W.-C.; Lei, H.; Chen, Z.; Luo, Z.-H. Review of machine learning for hydrodynamics, transport, and reactions in multiphase flows and reactors. *Ind. Eng. Chem. Res.* **2022**, *61*, 9901–9949. [CrossRef]
82. Kim, Y.; Park, H. Deep learning-based automated and universal bubble detection and mask extraction in complex two-phase flows. *Sci. Rep.* **2021**, *11*, 11. [CrossRef] [PubMed]
83. Shen, C.; Zheng, Q.; Shang, M.; Zha, L.; Su, Y. Using deep learning to recognize liquid–liquid flow patterns in microchannels. *AIChE J.* **2020**, *66*, e16260. [CrossRef]
84. Babanezhad, M.; Nakhjiri, A.T.; Marjani, A.; Shirazian, S. Pattern recognition of the fluid flow in a 3D domain by combination of Lattice Boltzmann and ANFIS methods. *Sci. Rep.* **2020**, *10*, 13. [CrossRef]
85. Yao, L.; Ou, Z.; Luo, B.; Xu, C.; Chen, Q. Machine Learning to Reveal Nanoparticle Dynamics from Liquid-Phase TEM Videos. *ACS Cent. Sci.* **2020**, *6*, 1421–1430. [CrossRef]

86. Brunton, S.L.; Hemati, M.S.; Taira, K. Special issue on machine learning and data-driven methods in fluid dynamics. *Theor. Comput. Fluid Dyn.* **2020**, *34*, 333–337. [CrossRef]
87. Manjrekar, O.N.; Dudukovic, M.P. Identification of flow regime in a bubble column reactor with a combination of optical probe data and machine learning technique. *Chem. Eng. Sci. X* **2019**, *2*, 100023. [CrossRef]
88. Mask, G.; Wu, X.; Ling, K. An improved model for gas-liquid flow pattern prediction based on machine learning. *J. Pet. Sci. Eng.* **2019**, *183*, 106370. [CrossRef]
89. Liu, L.; Bai, B. Flow regime identification of swirling gas-liquid flow with image processing technique and neural networks. *Chem. Eng. Sci.* **2019**, *199*, 588–601. [CrossRef]
90. Zhang, Y.; Azman, A.N.; Xu, K.-W.; Kang, C.; Kim, H.-B. Two-phase flow regime identification based on the liquid-phase velocity information and machine learning. *Exp. Fluid.* **2020**, *61*, 16. [CrossRef]
91. Pishnamazi, M.; Babanezhad, M.; Nakhjiri, A.T.; Rezakazemi, M.; Marjani, A.; Shirazian, S. ANFIS grid partition framework with difference between two sigmoidal membership functions structure for validation of nanofluid flow. *Sci. Rep.* **2020**, *10*, 15395. [CrossRef] [PubMed]
92. Barjouei, H.S.; Ghorbani, H.; Mohamadian, N.; Wood, D.A.; Davoodi, S.; Moghadasi, J.; Saberi, H. Prediction performance advantages of deep machine learning algorithms for two-phase flow rates through wellhead chokes. *J. Pet. Explor. Prod. Technol.* **2021**, *11*, 1233–1261. [CrossRef]
93. Kadish, S.; Schmid, D.; Son, J.; Boje, E. Computer Vision-Based Classification of Flow Regime and Vapor Quality in Vertical Two-Phase Flow. *Sensors* **2022**, *22*, 996. [CrossRef]
94. Kumar, P.; Sinha, K.; Nere, N.K.; Shin, Y.; Ho, R.; Mlinar, L.B.; Sheikh, A.Y. A machine learning framework for computationally expensive transient models. *Sci. Rep.* **2020**, *10*, 11492. [CrossRef]
95. Schäfer, B.; Beck, C.; Rhys, H.; Soteriou, H.; Jennings, P.; Beechey, A.; Heppell, C.M. Machine learning approach towards explaining water quality dynamics in an urbanised river. *Sci. Rep.* **2022**, *12*, 15. [CrossRef]
96. Loyola-Fuentes, J.; Pietrasanta, L.; Marengo, M.; Coletti, F. Machine Learning Algorithms for Flow Pattern Classification in Pulsating Heat Pipes. *Energies* **2022**, *15*, 1970. [CrossRef]
97. Zhang, J.; Zhang, S.; Zhang, J.; Wang, Z. Machine Learning Model of Dimensionless Numbers to Predict Flow Patterns and Droplet Characteristics for Two-Phase Digital Flows. *Appl. Sci.* **2021**, *11*, 4251. [CrossRef]
98. Ooi, Z.J.; Zhu, L.; Bottini, J.L.; Brooks, C.S. Identification of flow regimes in boiling flows in a vertical annulus channel with machine learning techniques. *Int. J. Heat Mass Transf.* **2021**, *185*, 122439. [CrossRef]
99. Arief, H.A.; Wiktorski, T.; Thomas, P.J. A Survey on Distributed Fibre Optic Sensor Data Modelling Techniques and Machine Learning Algorithms for Multiphase Fluid Flow Estimation. *Sensors* **2021**, *21*, 2801. [CrossRef]
100. Han, D.; Kwon, S. Application of Machine Learning Method of Data-Driven Deep Learning Model to Predict Well Production Rate in the Shale Gas Reservoirs. *Energies* **2021**, *14*, 3629. [CrossRef]
101. Manshadi, M.D.; Ghassemi, M.; Mousavi, S.; Mosavi, A.; Kovacs, L. Predicting the Parameters of Vortex Bladeless Wind Turbine Using Deep Learning Method of Long Short-Term Memory. *Energies* **2021**, *14*, 4867. [CrossRef]
102. Pan, D.; Yang, G.; Abo-Dief, H.M.; Dong, J.; Su, F.; Liu, C.; Li, Y.; Bin Xu, B.; Murugadoss, V.; Naik, N.; et al. Vertically Aligned Silicon Carbide Nanowires/Boron Nitride Cellulose Aerogel Networks Enhanced Thermal Conductivity and Electromagnetic Absorbing of Epoxy Composites. *Nano-Micro Lett.* **2022**, *14*, 118. [CrossRef]
103. Xu, Z.; Wu, F.; Yang, X.; Li, Y. Measurement of Gas-Oil Two-Phase Flow Patterns by Using CNN Algorithm Based on Dual ECT Sensors with Venturi Tube. *Sensors* **2020**, *20*, 1200. [CrossRef]
104. Roshani, M.; Phan, G.T.; Ali, P.J.M.; Roshani, G.H.; Hanus, R.; Duong, T.; Corniani, E.; Nazemi, E.; Kalmoun, E.M. Evaluation of flow pattern recognition and void fraction measurement in two phase flow independent of oil pipeline's scale layer thickness. *Alex. Eng. J.* **2021**, *60*, 1955–1966. [CrossRef]
105. Shanthi, C.; Pappa, N.; Suganya, J.A. Digital Image Processing Based Flow Regime Identification of Gas/Liquid Two—Phase Flow. *IFAC Proc. Vol.* **2013**, *46*, 409–414. [CrossRef]
106. Masood, H.; Farooq, H. Utilizing Spatio Temporal Gait Pattern and Quadratic SVM for Gait Recognition. *Electronics* **2022**, *11*, 2386. [CrossRef]
107. Rasel, R.K.; Chowdhury, S.M.; Marashdeh, Q.M.; Teixeira, F.L. Review of Selected Advances in Electrical Capacitance Volume Tomography for Multiphase Flow Monitoring. *Energies* **2022**, *15*, 5285. [CrossRef]
108. Zhu, L.; Xiao, X.; Wu, D.; Wang, Y.; Qing, X.; Xue, W. Qualitative Classification of Lubricating Oil Wear Particle Morphology Based on Coaxial Capacitive Sensing Network and SVM. *Sensors* **2022**, *22*, 6653. [CrossRef]
109. Carvalho, V.; Gonçalves, I.; Souza, A.; Souza, M.; Bento, D.; Ribeiro, J.; Lima, R.; Pinho, D. Manual and Automatic Image Analysis Segmentation Methods for Blood Flow Studies in Microchannels. *Micromachines* **2021**, *12*, 317. [CrossRef]
110. Chen, X.; Liang, H.; Li, Y.; Chen, D.; Wang, J.; Chen, J. Development of an Imaging and Impedance Flow Cytometer Based on a Constriction Microchannel and Deep Neural Pattern Recognition. *IEEE Trans. Electron Devices* **2022**, *69*, 6408–6416. [CrossRef]
111. Gao, Z.; Qu, Z.; Cai, Q.; Hou, L.; Liu, M.; Yuan, T. A Deep Branch-Aggregation Network for Recognition of Gas–Liquid Two-Phase Flow Structure. *IEEE Trans. Instrum. Meas.* **2020**, *70*, 8. [CrossRef]
112. Bediako, E.G.; Dančová, P.; Vít, T. Flow Boiling Heat Transfer of R134a in a Horizontal Smooth Tube: Experimental Results, Flow Patterns, and Assessment of Correlations. *Energies* **2022**, *15*, 7503. [CrossRef]

113. Kang, D.; Lee, J.; Chakraborty, A.; Lee, S.-E.; Kim, G.; Yu, C. Recent Advances in Two-Phase Immersion Cooling with Surface Modifications for Thermal Management. *Energies* **2022**, *15*, 1214. [CrossRef]
114. Suh, Y.; Bostanabad, R.; Won, Y. Deep learning predicts boiling heat transfer. *Sci. Rep.* **2021**, *11*, 10. [CrossRef]
115. Zhu, G.; Wen, T.; Zhang, D. Machine learning based approach for the prediction of flow boiling/condensation heat transfer performance in mini channels with serrated fins. *Int. J. Heat Mass Transf.* **2020**, *166*, 120783. [CrossRef]
116. Rokoni, A.; Zhang, L.; Soori, T.; Hu, H.; Wu, T.; Sun, Y. Learning new physical descriptors from reduced-order analysis of bubble dynamics in boiling heat transfer. *Int. J. Heat Mass Transf.* **2022**, *186*, 122501. [CrossRef]
117. He, Y.; Hu, C.; Li, H.; Hu, X.; Tang, D. Reliable predictions of bubble departure frequency in subcooled flow boiling: A machine learning-based approach. *Int. J. Heat Mass Transf.* **2022**, *195*, 123217. [CrossRef]
118. Zajec, B.; Cizelj, L.; Končar, B. Experimental Analysis of Flow Boiling in Horizontal Annulus—The Effect of Heat Flux on Bubble Size Distributions. *Energies* **2022**, *15*, 2187. [CrossRef]
119. Galicia, E.; Otomo, Y.; Saiwai, T.; Takita, K.; Orito, K.; Enoki, K. Subcooled Flow Boiling Heat Flux Enhancement Using High Porosity Sintered Fiber. *Appl. Sci.* **2021**, *11*, 5883. [CrossRef]